Structure of Sr-substituted photosystem II at 2.1 Å resolution and its implications in the mechanism of water oxidation

Faisal Hammad Mekky Koua[a,1], Yasufumi Umena[b,1,2,3], Keisuke Kawakami[c,2], and Jian-Ren Shen[a,4]

[a]Division of Bioscience, Graduate School of Natural Science and Technology/Faculty of Science, Okayama University, Okayama 700-8530, Japan; [b]Research Center for State-of-the-Art Functional Protein Analysis, Institute of Protein Research, Osaka University, Suita, Osaka 565-0871, Japan; and [c]Department of Chemistry, Graduate School of Science, Osaka City University, Sumiyoshi, Osaka 558-8585, Japan

Edited by Harry B. Gray, California Institute of Technology, Pasadena, CA, and approved February 1, 2013 (received for review November 17, 2012)

Oxygen-evolving complex of photosystem II (PSII) is a tetramanganese calcium penta-oxygenic cluster (Mn_4CaO_5) catalyzing light-induced water oxidation through several intermediate states (S-states) by a mechanism that is not fully understood. To elucidate the roles of Ca^{2+} in this cluster and the possible location of water substrates in this process, we crystallized Sr^{2+}-substituted PSII from *Thermosynechococcus vulcanus*, analyzed its crystal structure at a resolution of 2.1 Å, and compared it with the 1.9 Å structure of native PSII. Our analysis showed that the position of Sr was moved toward the outside of the cubane structure of the Mn_4CaO_5-cluster relative to that of Ca^{2+}, resulting in a general elongation of the bond distances between Sr and its surrounding atoms compared with the corresponding distances in the Ca-containing cluster. In particular, we identified an apparent elongation in the bond distance between Sr and one of the two terminal water ligands of Ca^{2+}, W3, whereas that of the Sr-W4 distance was not much changed. This result may contribute to the decrease of oxygen evolution upon Sr^{2+}-substitution, and suggests a weak binding and rather mobile nature of this particular water molecule (W3), which in turn implies the possible involvement of this water molecule as a substrate in the O-O bond formation. In addition, the PsbY subunit, which was absent in the 1.9 Å structure of native PSII, was found in the Sr-PSII structure.

membrane protein | water-splitting | structural changes | cyanobacteria | artificial photosynthesis

Photosynthetic light-induced water-splitting produces electrons, protons, and molecular oxygen from water; the latter product maintains the oxygenic atmosphere indispensable for sustaining oxygenic life on the earth. This process takes place in photosystem II (PSII), a multisubunit membrane protein complex containing 20 subunits with an overall molecular mass of 350 kDa (1, 2). In PSII, light is absorbed by the reaction center chlorophyll *a* molecules (P680), which initiates a series of electron transfer reactions leading to the formation of the charge separated state P_{680}^{+}/Q_A^{-} (the first quinone acceptor of PSII). The oxidized reaction center chlorophyll is rapidly reduced by a redox active tyrosine (Y_Z), which is the Tyr161 residue of the D1 protein. Subsequently, the oxidized Y_Z abstracts an electron from an oxygen-evolving complex (OEC), which is located close to Y_Z. Upon abstraction of four electrons from OEC, two water molecules are split into protons and molecular oxygen. Thus, the structure of OEC cycles through five distinct states termed S_i (where i = 0–4), with the S_0-state being the most reduced one, and the S_4-state a transit one. Among these S-states, the S_1-state is dark stable, and the molecular oxygen is produced in the transition of S_3-(S_4)-S_0 (3).

To understand the mechanism of photo-induced water-splitting, extensive studies have been carried out to reveal the structure of OEC (4–10). From these studies, it has been clear that the OEC is composed of four Mn and one Ca atoms, designated as the Mn_4Ca-cluster. Early crystallographic studies have shown the overall shape of this cluster (4–8). However, because of the limited resolution, the detailed structure of the Mn_4Ca-cluster remained unclear until the 1.9 Å resolution structure of PSII was reported in 2011 (11, 12). The high-resolution structural analysis revealed that the OEC contains five oxygens in addition to the four Mn and one Ca atoms, forming a Mn_4CaO_5-cluster, and they are arranged in a distorted chair form. In this chair form, three Mn, one Ca, and four oxygens form a cubane-like structure, whereas the fourth Mn (designated Mn4) is located outside of the cubane and associated with the cubic structure by μ-oxo-bridges. Four water molecules were found to serve as the terminal ligands to the metal cluster, among which, two are ligated to the fourth Mn and two to the Ca atom. Thus, at least some of these water molecules have been suggested to serve as the substrate for water-splitting (11–13).

The involvement of Ca in the Mn_4CaO_5-cluster and the presence of two water ligands to the Ca ion suggested an important role of this ion in water-splitting. Indeed, various previous studies have indicated the importance of Ca for water-splitting activity. Removal of Ca from higher plant PSII blocked the S-state transition beyond S_2-state, resulting in a complete loss of the oxygen-evolving activity (14–18). Among various other cations, only Sr^{2+} was shown to be able to partially replace the role of Ca^{2+}, resulting in an OEC with approximately half of the activity compared with that having Ca^{2+}-associated activity (15, 17–20). Similar results were obtained with cyanobacteria, where Ca^{2+} cannot be removed and replaced in isolated PSII so that it has to be replaced by Sr^{2+} in culture medium (21, 22). Substitution of Ca^{2+} with Sr^{2+} modifies the EPR properties of the S_2-state (15, 23) and alters several carboxylate-stretching modes of the S_2-S_1 FTIR difference spectrum (24–26). These results imply that Sr^{2+} substitution for Ca^{2+} perturbs the structure of the Mn_4CaO_5-cluster only slightly, suggesting that Ca^{2+} plays more than a structural role in the water-splitting reaction. Indeed, detailed extended X-ray absorption fine-structure (EXAFS) and multifrequency EPR studies have shown that the geometric and electronic structure of Mn_4CaO_5 and Mn_4SrO_5 are very similar (27–29). Isotope-exchange experiments using ^{18}O labeled water showed that, among the two exchangeable water molecules (30, 31), Sr^{2+}-substitution accelerated the exchange rate of a slowly exchanging water molecule by a factor of 3–4 (32). These results were taken as evidence to suggest that Ca^{2+} binds one of the substrate water molecules, and

Author contributions: F.H.M.K. and J.-R.S. designed research; F.H.M.K., Y.U., and K.K. performed research; Y.U. analyzed data; and F.H.M.K. and J.-R.S. wrote the paper.

The authors declare no conflict of interest.

This article is a PNAS Direct Submission.

Data deposition: The atomic coordinates and structure factors have been deposited in the Protein Data Bank, www.pdb.org (PDB ID code 4IL6).

[1]F.H.M.K. and Y.U. contributed equally to this work.

[2]Present address: The Osaka City University Advanced Research Institute for Natural Science and Technology, Osaka City University, Sumiyoshi, Osaka 558-8585, Japan.

[3]Present address: Chemical Conversion of Light Energy Group, Precursory Research for Embryonic Science and Technology, Japan Science and Technology Agency, Tokyo 102-0076, Japan.

[4]To whom correspondence should be addressed. E-mail: shen@cc.okayama-u.ac.jp.

This article contains supporting information online at www.pnas.org/lookup/suppl/doi:10.1073/pnas.1219922110/-/DCSupplemental.

substitution by Sr^{2+} affected the binding of this water, thereby decreasing the oxygen-evolving activity. The exact location of the substrate water molecules and the effects of Sr^{2+} replacement, however, are not clear at present.

Previously, attempts have been made to analyze the crystal structure of PSII with Ca^{2+} replaced by Sr^{2+} from a thermophilic cyanobacterium *Thermosynechococcus elongatus* (33). However, because of the low resolution (6.5 Å) of the crystals, the structure obtained did not allow an answer as to the structural changes induced by Sr^{2+}-substitution. In this study, we substituted Ca^{2+} by Sr^{2+} biosynthetically in the cells of *Thermosynechococus vulcanus*, and successfully crystallized and analyzed the Sr-PSII structure at a resolution of 2.1 Å. Our structure revealed several differences in the Mn_4Sr/CaO_5 cluster and its ligand environment. We also confirmed that the PsbY subunit, which was absent in the native structure of 1.9 Å resolution, was present in one of the monomers in the Sr^{2+}-subsituted PSII. Based on the comparison of Sr^{2+}-PSII structure with the native structure, we discuss possible mechanisms of photosynthetic water oxidation.

Results

Sr^{2+}-Substituted PSII and Its Crystallization. Although Ca^{2+} in the Mn_4CaO_5-cluster can be replaced by Sr^{2+} easily in purified PSII from higher plants, Ca^{2+} in cyanobacterial PSII cannot be removed and replaced by Sr^{2+} easily, and it has to be substituted by Sr^{2+} biosynthetically. Thus, we substituted Ca^{2+} with Sr^{2+} in the culture medium of *T. vulcanus*, and purified Sr^{2+}-substituted PSII according to the protocols reported previously (21, 22). In agreement with the previous reports, the cells appeared to grow in the Sr^{2+}-containing medium slightly slower than those in Ca^{2+}-containing medium, and the oxygen-evolving activity of purified Sr^{2+}-PSII dimer was lower by 40–50% than those of the Ca^{2+}-PSII dimer (Table 1). Nevertheless, the Sr^{2+}-PSII dimers obtained are of similar purity and homogeneity to those of Ca^{2+}-PSII dimers as analyzed by native and denatured electrophoresis (Fig. S1), which ensured the success of crystallization.

Crystals of Sr^{2+}-PSII dimers were obtained with similar conditions to those of Ca^{2+}-PSII dimers, except in the presence of Sr^{2+} in place of Ca^{2+}, and the diffraction data were collected with the X-rays of SPring-8 and processed to a resolution of 2.1 Å. As shown in Table S1, the space group of Sr^{2+}-PSII crystals is the same as that of Ca^{2+}-PSII, and the unit cell dimensions are also very similar between the two types of crystals. The structure was solved by the molecular replacement method with the native PSII structure (PDB ID 3ARC) (11) as the search model, which resulted in R_{work}/R_{free} factors of 17.6/20.5, and a Cruickshank diffraction-component precision index of 0.147 Å (34). This result yields an estimated standard uncertainty of 0.21 Å for bond distances in the overall structure, allowing us to compare the structure between Sr^{2+}-substituted and Ca^{2+}-containing PSII in detail.

Table 1. Oxygen-evolving activities of Sr^{2+}-substituted PSII in different preparations in comparison with the corresponding Ca^{2+}-PSII

PSII or crystal	Oxygen-evolving activity (μmol O_2/mg chl a/h)*	%
LDAO-PSII†		
Ca-PSII	2,000 ± 200	100
Sr-PSII	910 ± 10	46
Dimeric PSII		
Ca-PSII	3,750 ± 360	100
Sr-PSII	2,360 ± 170	63
Redissolved crystals		
Ca-PSII	2,800 ± 130	75‡
Sr-PSII	2,080 ± 140	55‡

*The values are averages of three separate samples.
†LDAO-PSII designates crude PSII particles obtained by solubilization of thylakoid membranes with lauryldimethylamine-*N*-oxide.
‡Percentage of the redissolved microcrystals out of noncrystallized (liquid) Ca-PSII activity.

The overall structure of the Sr^{2+}-substituted PSII is essentially identical to the native PSII, with the exception that the PsbY subunit was present in one of the two monomers. The averaged B-factor of Sr-PSII was 37.7 $Å^2$, which was only slightly higher than the averaged B-factor of 35.2 $Å^2$ of the native PSII structure at 1.9 Å resolution, and an rmsd value of 0.26 Å was obtained for superimposition of the Cα atoms between Sr-PSII and Ca-PSII. No significant differences were found in the number and arrangement of the PSII cofactors and lipid molecules between the Sr^{2+}-PSII and the native 1.9 Å PSII structure.

Comparison Between the Structures of Sr^{2+}-Substituted and Ca^{2+}-Containing Mn_4CaO_5-Cluster. The electron-density map for the Mn_4SrO_5-cluster was well defined and each of the metal ions was well separated (Fig. 1*A*), allowing us to identify the positions of the individual atoms, although some uncertainties are inevitable regarding the positions of μ-oxo bridges because of the effect of strong density of the nearby metal ions. The anomalous diffraction data taken at a wavelength of 0.76 Å clearly showed the presence of Sr^{2+} in place of Ca^{2+} in the Mn_4SrO_5-cluster (Fig. 1*B*). The occupancy of Sr^{2+} was estimated to be around 0.7, as can be seen from the somewhat lower electron density of Sr^{2+} than those of the Mn ions (Fig. 1*A*), despite the larger number of 36 electrons that Sr^{2+} has compared with the 21–22 electrons that Mn(III) or Mn (IV) have. This finding is consistent with earlier reports for a lower occupancy of Sr^{2+} in Sr^{2+}-substituted PSII (25, 35, 36). Although this may also bring a somewhat lower occupancy for W3 and W4, two water molecules associated with Ca/Sr (see below), the position of them are not affected by the slightly lower occupancy. As can be expected from the functional assembly of OEC in the presence of Sr^{2+}, the overall shape of the Mn_4SrO_5-cluster is very similar to that of the Mn_4CaO_5-cluster, which retained its characteristic, distorted chair form. The ligand environment of the Mn_4CaO_5-cluster was also retained in the Sr^{2+}-substituted OEC. A detailed comparison, however, revealed some important differences between the two structures, as described below.

The positions of the four Mn ions were essentially the same as those in native PSII (Fig. 1*C*), resulting in similar Mn-Mn distances in the Mn_4SrO_5-cluster as those of the Mn_4CaO_5 cluster (Fig. 2*A* and Table S2). The only slight differences found were in the average Mn1-Mn4 distance of two monomers, which was slightly (0.1 Å) longer, and in the average Mn3-Mn4 distance, which was slightly (0.1 Å) shorter, in the Mn_4SrO_5-cluster than those in the Mn_4CaO_5-cluster (Table S2). This result was because of a slight shift in the position of the dangler, Mn4 atom in the Mn_4SrO_5-cluster. However, we should point out that with the current level of resolution and the estimated standard uncertainty, it is difficult to conclude that these differences are significant.

The position of Sr^{2+} was shifted slightly more toward the outside of the cubane than that of Ca^{2+}, with an average distance of 0.3 Å between Sr-Ca from two monomers of Ca-containing PSII and Sr-containing PSII (Fig. 1*C* and Table S3). This shift resulted in a more distorted cubane structure, as well as a general elongation in the Sr-Mn distances compared with the Ca-Mn distances. Thus, the average distances of two monomers between Sr and Mn2-Mn4 were slightly (0.2 Å) longer than the corresponding Ca and Mn distances, and the Mn1-Sr distance was slightly (0.1 Å) longer than the Mn1-Ca distance (Fig. 2*B* and Table S3). These elongations can be ascribed to a larger ionic radius of Sr^{2+} (1.12 Å) than that of Ca^{2+} (0.99 Å). The resulting structure of the Mn_4SrO_5-cluster becomes more distorted, suggesting that it may be more unstable, which may account partially for the decrease in the oxygen-evolving activity upon substitution of Ca^{2+} by Sr^{2+}.

The positions of oxo-bridged oxygens were more difficult to determine accurately because the electron density of oxygen atoms was much weaker than those of Mn and Sr ions, which

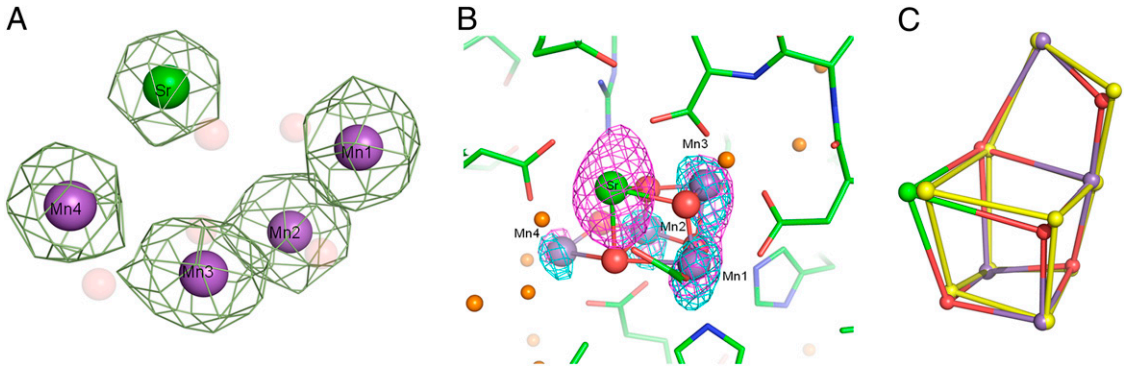

Fig. 1. Structure of the Mn_4SrO_5-cluster. (*A*) Assignment of each of the metal ions in the Mn_4SrO_5-cluster of Sr-PSII. Green meshes represent 2*Fo-Fc* map of the metal ions contoured at 7.0 σ. (*B*) Assignment of the position of Sr based on the anomalous difference map. Magenta: anomalous difference map (5 σ) taken at the peak wavelength of λ = 0.76 Å. Cyan: difference-Fourier map (5 σ) taken at the remote wavelength of λ = 0.80 Å. (*C*) Superimposition of the Mn_4SrO_5-cluster with the 1.9 Å Mn_4CaO_5 cluster (PBD ID 3ARC). Colored atoms represent the Mn_4SrO_5-cluster, and yellow atoms represent the Mn_4CaO_5-cluster.

hampered the determination of exact positions of each of the oxygen atoms. Thus, the positions of the five oxo-bridged oxygens may bear larger errors than other atoms in the structure refined to the 2.1 Å resolution. We located each of the oxygen atoms in the Mn_4SrO_5-cluster based on their omit-map. Superposition of the structure of the Mn_4SrO_5-cluster with that of the Mn_4CaO_5-cluster showed that most of the oxygen atoms are located in similar positions between the two structures (Fig. 1*C*), resulting in only slight differences in the bond-distances among Mn-O between Sr^{2+}-PSII and Ca^{2+}-PSII, which are mostly in the range of 0.1–0.2 Å (Fig. 2*C* and Table S2). Among these differences, some bonds became longer, whereas some became shorter, suggesting that at least some of these differences are caused by experimental errors. Another source of the differences may lie in the slightly lower occupancy of Sr^{2+}, as this may have led to a restricted structure of the Mn_4SrO_5 cluster slightly different from that of Mn_4CaO_5 during the refinement process. It is thus difficult to evaluate the possible consequences of these differences on the function of the metal cluster. Despite these consequences, we note that there were five Mn-O bonds that became 0.2 Å shorter and one bond that became 0.3 Å shorter, whereas only two bonds became 0.2 Å longer upon Sr^{2+} substitution (Table S2).

Among the bond-distances between Sr and oxo-bridges, O2-Sr became 0.2 Å longer, reflecting again the movement of Sr^{2+} relative to Ca^{2+}. On the other hand, the other O-Sr distances were not much changed compared with those of O-Ca distances (Fig. 2*C* and Table S3).

The four water molecules ligated to the Mn_4CaO_5-cluster were retained in the Mn_4SrO_5-cluster, and the positions of three (W1, W2, W4) of the four water molecules in the Mn_4SrO_5-cluster are similar to those in the Mn_4CaO_5-cluster (Figs. 2*C* and 3, and Table S3), resulting in bond-distances of W1-Mn4, W2-Mn4, and W4-Sr that are within 0.1 Å differences compared with those in the Mn_4CaO_5-cluster (Table S3). Importantly however, the position of W3 was shifted by 0.4–0.6 Å relative to its position in Ca-PSII in the two monomers (Table S3) upon Sr^{2+}-substitution, resulting in a bond-distance that was 0.2–0.3 Å longer (depending on which one of the two monomers are concerned) than the corresponding distance in the Mn_4CaO_5-cluster (Table S3). These differences exceeded the estimated standard uncertainty of the structure analyzed at the current resolution, and were also much larger than the shift in the position of W4 (0.2 Å) upon Sr^{2+}-substitution relative to its position in Ca-PSII. In fact, the bond length between W4-Sr was 2.3 Å in Sr^{2+}-substituted PSII, which was even slightly (0.1 Å) shorter than the bond length of W4-Ca in Ca^{2+}-containing PSII, whereas the average bond length of W3-Sr was 2.6 Å, suggesting a much weaker binding of W3 than that of W4 in Sr-PSII. Moreover, the shift in the position of W3 upon Sr^{2+}-substitution was the largest among those of the four water molecules. Although the resulted changes in the bond length of W3-Sr was still not large considering the current level of estimated standard uncertainty, we should point out that the lengthening in the bond distance between W3-Sr was observed in two PSII monomers, the structures of which were refined independently against the diffraction data, and we have confirmed this lengthening from three datasets collected from three independent crystals. These results suggested that the binding of W3 was specifically affected upon Sr^{2+}-substitution. Because of this effect, the distance

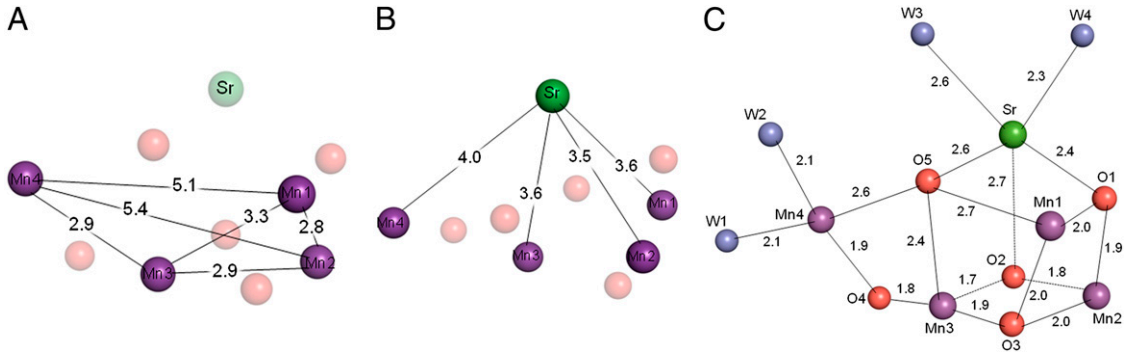

Fig. 2. Distances between the metal ions and between metal and oxo-ligands of the Mn_4SrO_5-cluster. (*A*) Average distances of two monomers between Mn-Mn in the Mn_4SrO_5-cluster. (*B*) Average distances between Mn-Sr in the Mn_4SrO_5-cluster. (*C*) Average distances between metal and oxo-ligands of the Mn_4SrO_5-cluster.

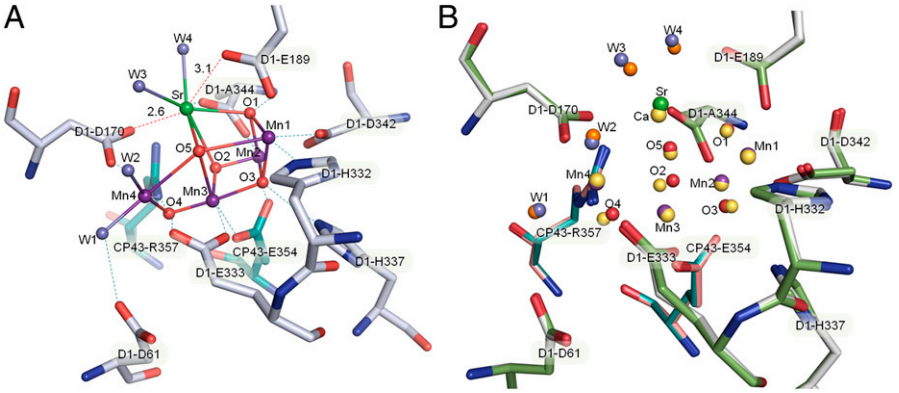

Fig. 3. Ligand environment of the Mn_4SrO_5-cluster. (*A*) Ligand structure of the Mn_4SrO_5-cluster in Sr-PSII. (*B*) Superimposition of the ligand structure of the Mn_4SrO_5-cluster with that of the Mn_4CaO_5-cluster.

between W2-W3 was changed from 3.3 Å to 3.5 Å, resulting in a weaker interaction between these two water molecules in Sr-PSII. These changes may contribute to the decrease in the oxygen-evolving activity and also the alterations in the EPR property of $S_iY_Z^{\cdot}$ states ($i = 0$ ~3) (15, 23) upon Sr^{2+}-substitution.

The ligand environment of the Mn_4CaO_5-cluster was essentially preserved in the Mn_4SrO_5-cluster (Fig. 3). Most of the bond-distances between the ligands and the metal ions were not changed in the Mn_4SrO_5-cluster. However, the side-chain of D1-Asp170 was shifted upon Sr^{2+}-substitution, resulting in an average Sr-D1-Asp170 distance of 2.6 Å, which is 0.2 Å longer than the corresponding distance in the Mn_4CaO_5-cluster (Fig. 3 and Table S3). On the other hand, the bond-distance between D1-Asp170 and Mn4 was not changed. Another difference was found in the distance of Sr-Glu189-D1, which was 0.2 Å shorter in the Mn_4SrO_5-cluster than that in the Mn_4CaO_5-cluster. Because D1-Asp170 is a bidentate ligand to Ca and Mn4, the elongation of the Sr-Asp170 distance apparently reflects the larger ionic radius of the Sr^{2+} compared with that of the Ca^{2+} ion, and may cause weaker binding of this residue to the Sr^{2+} ion. On the other hand, the distance of the carboxylate group of D1-Glu189 to Ca^{2+} is 3.3 Å in the native PSII structure, which indicates that D1-Glu189 is not a direct ligand to Ca^{2+}. However, the distance between D1-Glu189 and Sr^{2+} in Sr^{2+}-PSII became shorter (3.1 Å). This result suggests that the carboxylate group of D1-Glu189 may have a stronger interaction with Sr^{2+} than that with Ca^{2+}, which may partially compensate for the elongation in the distance of Sr-Asp170.

Additional Differences Between Sr^{2+}-Substituted and Native PSII. In addition to the differences found within or around the Mn_4CaO_5-cluster described above, some other differences were found in the regions not directly related to the Mn_4CaO_5-cluster. The PsbY subunit was found in one of the two monomers, which had a less crystal contact within the unit cell in the Sr^{2+}-substituted PSII. This subunit was present in two of the previous medium-resolution structures (5, 7, 8), and identified from a structural study with a deletion mutant (37), but was absent in the other structural studies reported previously, including the 1.9 Å resolution structure (4, 6, 11). These results suggested a weak binding of this subunit to PSII. Indeed, the electron-density map for this subunit found in the Sr^{2+}-PSII was weak and was absent in the other monomer. As a result, this subunit had a higher average *B*-factor compared with the other regions of PSII. From the resolved structure, PsbY was located in close proximity to the transmembrane helices of cyt *b*559 in the peripheral region of the complex, and appeared to have contacts only with the cyt *b*559 subunit in the complex (Fig. 4). The N-terminal region of PsbY was close to PsbE, where PsbY-Arg4 appeared to interact with PsbE-Gly41 and PsbE-Asp45. PsbY-Ala19 in the middle region was close to the heme molecule (HEM-641), whereas the C-terminal region of PsbY was close to PsbF, with PsbY-Gln30 possibly interacting with two residues from subunit PsbF (PsbF-Ile15 and PsbF-Phe16). The C-terminal region of the PsbY protein was also found to interact weakly with a lipid molecule (SQD-768). These results might explain the weak binding of this protein to PSII. Consistent with previous models, the N terminal of the PsbY helix is oriented toward the luminal side (37). The multiple sequence alignment for PsbY proteins showed that among the three residues involved in the helix–helix interactions, Arg4 and Gln30 are completely conserved, whereas Ala19 is conserved among cyanobacteria and red algae but replaced by Val in green algae and higher plants (Fig. S2).

In addition to the above differences, there were also some differences found in the region around Y_D, as well as the additional binding sites of Ca^{2+} and Cl^- between Sr-PSII and Ca-PSII. These differences are described in the *SI Results and Discussion* (Fig. S3).

Discussion

Extensive studies have been performed on the roles of Ca^{2+} in the oxygen-evolving reaction, and perturbations of the S-state transition have been well documented upon replacement of Ca^{2+} by Sr^{2+} (15–29). Substitution by Sr^{2+} slows down S-state transition beyond S_2 and S_3-states, leading to the formation of an S_2-state with somewhat different properties in terms of its redox potential, stability, and the EPR multiline signal (17–20, 22–26). However, because of the absence of detailed structural information, the exact role of Ca^{2+} and the causes underlying the effects of substitution by Sr^{2+} are not clear.

In this study, we analyzed the Sr^{2+}-substituted PSII structure to a resolution of 2.1 Å, which is much higher than the previously attained resolution of 6.5 Å (33). This analysis allowed us to compare the Sr^{2+}-substituted PSII structure with the native PSII structure in a much greater detail. As expected from the functional assembly of the Mn_4SrO_5-cluster, as well as from the previous detailed EXAFS (27) and multifrequency EPR studies (28), the overall structure of PSII and of the Mn_4SrO_5-cluster was very similar to that of the native PSII. The Mn-Mn and Mn-O distances in the Mn_4SrO_5-cluster were found to be largely similar to those in native PSII. The position of Sr^{2+}, however, was moved toward the outside of the cubane than that of Ca^{2+}. This finding is in agreement with the results from the previous EXAFS study (27), although the EXAFS study did not give information on the exact position of Sr^{2+}. In relation to this result, some significant differences were found: (*i*) Sr-Mn1 distance was slightly (0.1 Å) longer, and Sr-Mn2, Mn3, Mn4 distances were 0.2 Å longer than the corresponding Ca-Mn distances. (*ii*) Although Sr-O1, O3, O4, O5 distances were similar to those of the corresponding Ca-O distances, the Sr-O2 distance became 0.2 Å longer than the corresponding Ca-O distance. (*iii*) Although

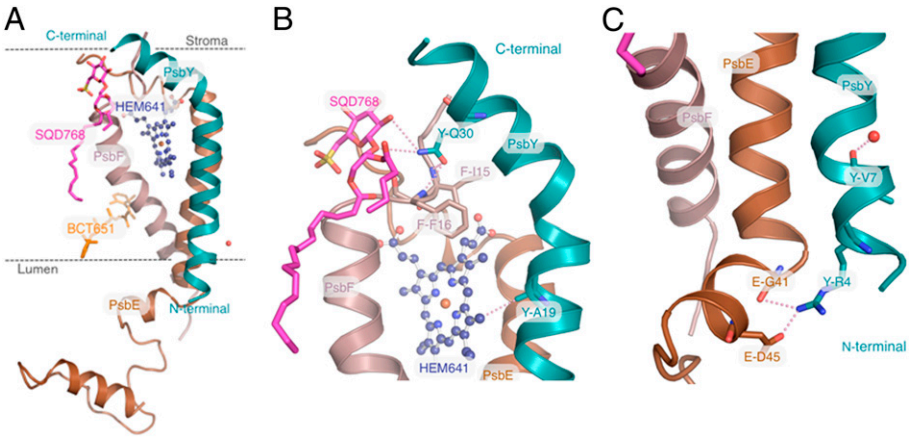

Fig. 4. Structure of the PsbY protein and its interacting subunits. (*A*) The PsbY protein (cyan) view perpendicular to the membrane normal plane, together with the nearby cyt_{559} subunits, PsbE (brown) and PsbF (pale violet). (*B*) Enlarged view of the C-terminal region of PsbY, showing the interactions of PsbY with PsbF and HEM-641. (*C*) Enlarged view of the N-terminal region showing interactions of PsbY with PsbE.

Sr-W4 distance was not much changed or even slightly (0.1 Å) shorter than the Ca-W4 distance, the Sr-W3 distance was elongated by 0.2–0.3 Å. In accordance with this, the distance of W2-W3 became longer, resulting in a weaker interaction between W2 and W3. (*iv*) Among the ligands to the Mn_4SrO_5-cluster, the distance of D1-Asp170-Sr became 0.2 Å longer, and that of D1-Glu189-Sr became 0.2 Å shorter.

Among the above differences, the elongation between the distances of (*i*) Sr-Mn, (*ii*) Sr-O2, and (*iv*) D1-Asp170-Sr is resulted from the movement of Sr^{2+} toward the outside of the cubane to the direction of D1-Glu189, relative to the position of Ca^{2+} (the distance between Sr and Ca was found to be 0.3 Å). This movement can be ascribed to a larger ionic radius of Sr^{2+} (1.12 Å) than that of Ca^{2+} (0.99 Å). The shorter distance between D1-Glu189 and Sr may be a result of the necessity to compensate for the elongation in the distance of D1-Asp170-Sr. The perturbations on caboxylate ligands of the Mn_4CaO_5-cluster upon Sr^{2+}-substitution have been reported previously by FTIR measurements (24–26), and these perturbations may reflect the shift of D1-Asp170 and D1-Glu189 observed here. Although these changes may contribute to the decrease in the oxygen-evolving activity, the change in the distance of one of the two water ligands (W3) to Sr^{2+} appears more significant: although the distance of W4-Sr^{2+} was similar or even somewhat shorter than that of W4-Ca^{2+}, the distance of W3-Sr^{2+} was elongated by 0.2–0.3 Å than that of W3-Ca^{2+}. These differences were observed in the two PSII monomers independently, and we have confirmed these differences from three independent crystals. This result cannot be explained by the movement of Sr^{2+} alone, and suggests that W3 is much mobile, or its binding is much weaker, than that of W4 in Sr^{2+}-PSII. In fact, the position of W3 was shifted by an average distance of 0.5 Å relative to its position in Ca-PSII upon substitution by Sr^{2+}, which is much larger than the shift in the position of W4 (0.2 Å), as well as the other two water molecules bound to Mn4 (W1, W2). Because of this change, the interaction between W2 and W3 found in native PSII became weaker. These changes may significantly contribute to the decrease in the oxygen-evolving activity, and may have significant mechanistic implications, as discussed below.

Previous isotope exchange studies have shown that, among the two exchangeable, substrate water molecules, Sr^{2+}-substitution accelerated the exchange rate of a slowly exchanging water molecule (32). Because Mn_4SrO_5 had a very similar geometric (27) and electronic (28) structure to that of Mn_4CaO_5, it has been suggested that Ca plays a functional role in binding substrate water molecules, rather than a structural role. The slowly exchanging water molecule affected by Sr^{2+}-substitution was thus considered to be bound to Ca^{2+} (28, 32). In the 1.9 Å structure of PSII, four water molecules were associated with the Mn_4CaO_5-cluster. Based on the weak binding of O5 to its nearby atoms, it has been suggested that O5 may form part of the site for O-O bond formation. Among the four water molecules, W2 ligated to Mn4 and W3 ligated to Ca^{2+} were found to be in hydrogen-bonding distances to O5; they were therefore proposed to provide at least part of the substrate water molecules. The weak binding and mobile feature of W3 revealed in the present study suggests that W3 may have a higher reactivity and more easily change its position during the reaction cycle. The significant elongation in the W3-Sr bond length also suggests that W3 may correspond to the "slowly exchanging" water identified by the isotope exchange experiments, and its exchange rate became faster because of the elongation in the bond distance between W3 and Sr^{2+} in Sr^{2+}-substituted PSII. This result points to the possibility that W3 may move closer to O5 at some stage of the S-state cycle, allowing the O-O bond formation among these two species. Indeed, the mechanism of O-O bond formation between a Ca-bound water/hydroxo and a Mn-bridged oxygen has been suggested from previous EXAFS and multifrequency EPR studies (27, 28).

The breakage of the hydrogen-bond between W2 and W3 in Sr^{2+}-substituted PSII may also lead to a fast exchange rate of W2, which in turn suggests that W2 may be involved in the O-O bond formation. In this case, the O-O bond formation may occur either between W2 and W3, or between W2 and O5. In either of these cases, we have assumed that the two substrate water molecules are already present in the dark-stable S_1-state, as suggested from the isotope-exchange experiments (38, 39). Because two water molecules have been suggested to be newly inserted during the S-state cycle (40, 41), the above suggestions assume that the newly inserted water molecules replace the bound water molecules and serve as substrates for the next reaction cycle. However, if we consider that one or two of the newly inserted water molecules already participate in the present reaction cycle, the O-O bond may be formed between W2, W3, or O5, and a newly inserted water molecule. In fact, the possibility of O-O bond formation between W3 or O5, and a newly inserted water molecule has been suggested from recent theoretical studies (42–46). In any cases, our present results showed that W4 was not affected by the Sr-substitution, suggesting that this water molecule binds rigidly to Ca^{2+}, and therefore may function as a structural water molecule rather than a substrate.

Materials and Methods

To substitute Ca^{2+} with Sr^{2+}, *T. vulcanus* cells were grown in a Ca-Free/Sr-containing medium as described in refs. 21 and 22. The growth was monitored by OD_{730nm} and photosynthetic activity. The thylakoid membranes and

Sr-PSII core dimer complexes were purified with the method of Shen and Inoue (47), with modifications as previously described (21, 22, 48). The Sr-PSII dimer compositions, activity, and homogeneity were assessed before each crystallization experiment. The purified Sr-PSII dimer was crystallized according to the conditions used for crystallizing Ca-PSII (11), with Sr^{2+} replacing Ca^{2+} in the crystallization buffer. The crystals obtained were frozen after substitution of the buffer with a cryo-protectant solution (11), and the X-ray diffraction data were collected at beamlines BL-44XU and BL-41XU of SPring-8 (Hyogo, Japan), with a slide-oscillation method described previously (11) that gave rise to a similar X-ray dose as that used for collecting the 1.9 Å dataset (see *SI Materials and Methods* for more details). Several full datasets were collected at Sr *K* absorption edge (0.76 Å) and remote (0.8 Å) wavelengths and processed to a resolution range of 2.1~2.5 Å. Another full dataset was collected at a wavelength of 1.75 Å and processed to a 2.6 Å resolution to examine the Ca^{2+} and Cl^{-} binding sites. Further details of the experimental procedures are described in *SI Materials and Methods*.

ACKNOWLEDGMENTS. The authors thank Dr. Nobuo Kamiya for his valuable help and suggestions in the structural analysis and discussion of the results; and the staff members at beamlines BL41XU and BL44XU of SPring-8, Japan, for their kind help in data collection. This work was supported by a Grant-in-Aid for Specially Promoted Research 24000018 from Ministry of Education, Culture, Sports, Science, and Technology/Japan Society for the Promotion of Science of Japan (to J.-R.S.). F.H.M.K. was supported by a scholarship from the Japanese government (Ministry of Education, Culture, Sports, Science, and Technology).

1. Wydrzynski TJ, Satoh K, eds (2005) *Photosystem II: The Light-Driven Water:Plastoquinone Oxidoreductase* (Springer, Dordrecht, The Netherlands).
2. Shen JR, Henmi T, Kamiya N (2008) Structure and Function of Photosystem II. *Structure of Photosynthetic Proteins*, ed Fromme P (Wiley, Weinheim, Germany), pp. 83–106.
3. Kok B, Forbush B, McGloin M (1970) Cooperation of charges in photosynthetic O2 evolution-I. A linear four step mechanism. *Photochem Photobiol* 11(6):457–475.
4. Zouni A, et al. (2001) Crystal structure of photosystem II from *Synechococcus elongatus* at 3.8 A resolution. *Nature* 409(6821):739–743.
5. Kamiya N, Shen JR (2003) Crystal structure of oxygen-evolving photosystem II from *Thermosynechococcus vulcanus* at 3.7-A resolution. *Proc Natl Acad Sci USA* 100(1): 98–103.
6. Ferreira KN, Iverson TM, Maghlaoui K, Barber J, Iwata S (2004) Architecture of the photosynthetic oxygen-evolving center. *Science* 303(5665):1831–1838.
7. Loll B, Kern J, Saenger W, Zouni A, Biesiadka J (2005) Towards complete cofactor arrangement in the 3.0 A resolution structure of photosystem II. *Nature* 438(7070): 1040–1044.
8. Guskov A, et al. (2009) Cyanobacterial photosystem II at 2.9-A resolution and the role of quinones, lipids, channels and chloride. *Nat Struct Mol Biol* 16(3):334–342.
9. Yano J, et al. (2006) Where water is oxidized to dioxygen: Structure of the photosynthetic Mn_4Ca cluster. *Science* 314(5800):821–825.
10. Siegbahn PE (2000) Theoretical models for the oxygen radical mechanism of water oxidation and of the water oxidizing complex of photosystem II. *Inorg Chem* 39(13): 2923–2935.
11. Umena Y, Kawakami K, Shen JR, Kamiya N (2011) Crystal structure of oxygen-evolving photosystem II at a resolution of 1.9 Å. *Nature* 473(7345):55–60.
12. Kawakami K, Umena Y, Kamiya N, Shen JR (2011) Structure of the catalytic, inorganic core of oxygen-evolving photosystem II at 1.9 Å resolution. *J Photochem Photobiol B* 104(1–2):9–18.
13. Rapatskiy L, et al. (2012) Detection of the water-binding sites of the oxygen-evolving complex of Photosystem II using W-band ^{17}O electron-electron double resonance-detected NMR spectroscopy. *J Am Chem Soc* 134(40):16619–16634.
14. Ono T, Inoue Y (1988) Discrete extraction of the Ca^{2+} atom functional for O_2 evolution in higher plant photosystem II by a simple low pH treatment. *FEBS Lett* 227(2): 147–152.
15. Boussac A, Rutherford AW (1988) Nature of the inhibition of the oxygen-evolving enzyme of photosystem II induced by NaCl washing and reversed by the addition of Ca^{2+} or Sr^{2+}. *Biochemistry* 27(9):3476–3483.
16. Sivaraja M, Tso J, Dismukes GC (1989) A calcium-specific site influences the structure and activity of the manganese cluster responsible for photosynthetic water oxidation. *Biochemistry* 28(24):9459–9464.
17. Ono T-A, Rompel A, Mino H, Chiba N (2001) $Ca^{(2+)}$ function in photosynthetic oxygen evolution studied by alkali metal cations substitution. *Biophys J* 81(4):1831–1840.
18. Vrettos JS, Stone DA, Brudvig GW (2001) Quantifying the ion selectivity of the Ca^{2+} site in photosystem II: Evidence for direct involvement of Ca^{2+} in O_2 formation. *Biochemistry* 40(26):7937–7945.
19. Yocum CF (2008) The calcium and chloride requirements of the O_2 evolving complex. *Coord Chem Rev* 252(3–4):296–305.
20. Yachandra VK, Yano J (2011) Calcium in the oxygen-evolving complex: Structural and mechanistic role determined by X-ray spectroscopy. *J Photochem Photobiol B* 104(1–2):51–59.
21. Boussac A, et al. (2004) Biosynthetic Ca^{2+}/Sr^{2+} exchange in the photosystem II oxygen-evolving enzyme of *Thermosynechococcus elongatus*. *J Biol Chem* 279(22):22809–22819.
22. Ishida N, et al. (2008) Biosynthetic exchange of bromide for chloride and strontium for calcium in the photosystem II oxygen-evolving enzymes. *J Biol Chem* 283(19): 13330–13340.
23. Westphal KL, Lydakis-Simantiris N, Cukier RI, Babcock GT (2000) Effects of Sr2+-substitution on the reduction rates of Yz* in PSII membranes—Evidence for concerted hydrogen-atom transfer in oxygen evolution. *Biochemistry* 39(51):16220–16229.
24. Kimura Y, Hasegawa K, Ono TA (2002) Characteristic changes of the S_2/S_1 difference FTIR spectrum induced by Ca^{2+} depletion and metal cation substitution in the photosynthetic oxygen-evolving complex. *Biochemistry* 41(18):5844–5853.
25. Strickler MA, Walker LM, Hillier W, Debus RJ (2005) Evidence from biosynthetically incorporated strontium and FTIR difference spectroscopy that the C-terminus of the D1 polypeptide of photosystem II does not ligate calcium. *Biochemistry* 44(24): 8571–8577.
26. Suzuki H, Taguchi Y, Sugiura M, Boussac A, Noguchi T (2006) Structural perturbation of the carboxylate ligands to the manganese cluster upon Ca^{2+}/Sr^{2+} exchange in the S-state cycle of photosynthetic oxygen evolution as studied by flash-induced FTIR difference spectroscopy. *Biochemistry* 45(45):13454–13464.
27. Pushkar Y, Yano J, Sauer K, Boussac A, Yachandra VK (2008) Structural changes in the Mn_4Ca cluster and the mechanism of photosynthetic water splitting. *Proc Natl Acad Sci USA* 105(6):1879–1884.
28. Cox N, et al. (2011) Effect of Ca^{2+}/Sr^{2+} substitution on the electronic structure of the oxygen-evolving complex of photosystem II: A combined multifrequency EPR, ^{55}Mn-ENDOR, and DFT study of the S_2 state. *J Am Chem Soc* 133(10):3635–3648.
29. Rappaport F, Ishida N, Sugiura M, Boussac A (2011) Ca^{2+} determines the entropy changes associated with the formation of transition states during water oxidation by Photosystem II. *Energy Environ Sci* 4(7):2520–2524.
30. Messinger J, Badger M, Wydrzynski T (1995) Detection of one slowly exchanging substrate water molecule in the S3 state of photosystem II. *Proc Natl Acad Sci USA* 92(8):3209–3213.
31. Hillier W, Wydrzynski T (2000) The affinities for the two substrate water binding sites in the $O_{(2)}$ evolving complex of photosystem II vary independently during S-state turnover. *Biochemistry* 39(15):4399–4405.
32. Hendry G, Wydrzynski T (2003) (^{18}O isotope exchange measurements reveal that calcium is involved in the binding of one substrate-water molecule to the oxygen-evolving complex in photosystem II. *Biochemistry* 42(20):6209–6217.
33. Kargul J, et al. (2007) Purification, crystallization and X-ray diffraction analyses of the *T. elongatus* PSII core dimer with strontium replacing calcium in the oxygen-evolving complex. *Biochim Biophys Acta* 1767(6):404–413.
34. Cruickshank DWJ (1999) Remarks about protein structure precision. *Acta Crystallogr D Biol Crystallogr* 55(Pt 3):583–601.
35. Yano J, et al. (2011) Altered structure of the Mn4Ca cluster in the oxygen-evolving complex of photosystem II by a histidine ligand mutation. *J Biol Chem* 286(11): 9257–9267.
36. Boussac A, Sugiura M, Lai TL, Rutherford AW (2008) Low-temperature photochemistry in photosystem II from *Thermosynechococcus elongatus* induced by visible and near-infrared light. *Philos Trans R Soc Lond B Biol Sci* 363(1494):1203–1210, discussion 1210.
37. Kawakami K, Iwai M, Ikeuchi M, Kamiya N, Shen JR (2007) Location of PsbY in oxygen-evolving photosystem II revealed by mutagenesis and X-ray crystallography. *FEBS Lett* 581(25):4983–4987.
38. Hendry G, Wydrzynski T (2002) The two substrate-water molecules are already bound to the oxygen-evolving complex in the S_2 state of photosystem II. *Biochemistry* 41(44): 13328–13334.
39. Hillier W, Wydrzynski T (2004) Substrate water interactions within the Photosystem II oxygen evolving complex. *Phys Chem Chem Phys* 6(20):4882–4889.
40. Noguchi T, Sugiura M (2000) Structure of an active water molecule in the water-oxidizing complex of photosystem II as studied by FTIR spectroscopy. *Biochemistry* 39(36):10943–10949.
41. Noguchi T (2008) FTIR detection of water reactions in the oxygen-evolving centre of photosystem II. *Philos Trans R Soc Lond B Biol Sci* 363(1494):1189–1194, discussion 1194–1195.
42. Yamanaka S, et al. (2011) Possible mechanisms for the O-O bond formation in oxygen evolution reaction at the $CaMn_4O_5(H_2O)_4$ cluster of PSII refined to 1.9 A X-ray resolution. *Chem Phys Lett* 511(1–3):138–145.
43. Isobe H, et al. (2012) Theoretical illumination of water-inserted structures of the CaMn4O5 cluster in the S_2 and S_3 states of oxygen-evolving complex of photosystem II: Full geometry optimizations by B3LYP hybrid density functional. *Dalton Trans* 41(44):13727–13740.
44. Siegbahn PEM (2008) A structure-consistent mechanism for dioxygen formation in photosystem II. *Chemistry* 14(27):8290–8302.
45. Siegbahn PEM (2009) Structures and energetics for O_2 formation in photosystem II. *Acc Chem Res* 42(12):1871–1880.
46. Siegbahn PEM (2012) Mechanisms for proton release during water oxidation in the S_2 to S_3 and S_3 to S_4 transitions in photosystem II. *Phys Chem Chem Phys* 14(14):4849–4856.
47. Shen JR, Inoue Y (1993) Binding and functional properties of two new extrinsic components, cytochrome c-550 and a 12-kDa protein, in cyanobacterial photosystem II. *Biochemistry* 32(7):1825–1832.
48. Shen JR, Kamiya N (2000) Crystallization and the crystal properties of the oxygen-evolving photosystem II from *Synechococcus vulcanus*. *Biochemistry* 39(48): 14739–14744.